

# Three-dimensional susceptibility-weighted imaging and two-dimensional T2\*-weighted gradient-echo imaging of intratumoral hemorrhages in pediatric diffuse intrinsic pontine glioma

Ulrike Löbel · Jan Sedlacik · Noah D. Sabin · Mehmet Kocak · Alberto Broniscer · Claudia M. Hillenbrand · Zoltán Patay

Received: 2 February 2010 / Accepted: 3 September 2010 / Published online: 28 September 2010  
© Springer-Verlag 2010

## Abstract

**Introduction** We compared the sensitivity and specificity of T2\*-weighted gradient-echo imaging (T2\*-GRE) and susceptibility-weighted imaging (SWI) in determining prevalence and cumulative incidence of intratumoral hemorrhages in children with diffuse intrinsic pontine glioma (DIPG) undergoing antiangiogenic and radiation therapy. **Methods** Patients were recruited from an institutional review board-approved prospective phase I trial of vandetanib administered in combination with radiation therapy. Patient consent was obtained before enrollment. Consecutive T2\*-GRE and SWI exams of 17 patients (F/M: 9/8; age 3–17 years) were evaluated. Two reviewers (R1 and R2) determined the number and size of hemorrhages at baseline and multiple follow-ups (92 scans, mean 5.4/patient). Statistical analyses were performed using descriptive statistics, graphical tools, and mixed-effects Poisson regression models.

**Results** Prevalence of hemorrhages at diagnosis was 41% and 47%; the cumulative incidences of hemorrhages at 6 months by T2\*-GRE and SWI were 82% and 88%, respectively. Hemorrhages were mostly petechial; 9.7% of lesions on T2\*-GRE and 5.2% on SWI were hematomas (>5 mm). SWI identified significantly more hemorrhages than T2\*-GRE did. Lesions were missed or misinterpreted in 36/39 (R1/R2) scans by T2\*-GRE and 9/3 scans (R1/R2) by SWI. Hemorrhages had no clinically significant neurological correlates in patients.

**Conclusions** SWI is more sensitive than T2\*-GRE in detecting hemorrhages and differentiating them from calcification, necrosis, and artifacts. Also, petechial hemorrhages are more common in DIPG at diagnosis than previously believed and their number increases during the course of treatment; hematomas are rare.

**Keywords** T2\*-weighted gradient-echo imaging · Susceptibility-weighted imaging · Pediatric · Diffuse intrinsic pontine glioma · Hemorrhage

U. Löbel · J. Sedlacik · N. D. Sabin · C. M. Hillenbrand · Z. Patay (✉)  
Department of Radiological Sciences,  
St. Jude Children's Research Hospital,  
262 Danny Thomas Place, Mail Stop 220,  
Memphis, TN 38105, USA  
e-mail: zoltan.patay@stjude.org

M. Kocak  
Department of Biostatistics,  
St. Jude Children's Research Hospital,  
262 Danny Thomas Place,  
Memphis, TN 38105, USA

A. Broniscer  
Department of Oncology, St. Jude Children's Research Hospital,  
262 Danny Thomas Place,  
Memphis, TN 38105, USA

## Introduction

Brainstem tumors represent 2% of primary central nervous system (CNS) tumors and account for 12% of cerebral neoplasms in children [1, 2]. A subset of these patients with focal lesions (20%) have good prognosis [3]. However, the outcome of patients with diffuse intrinsic pontine glioma (DIPG) remains grim [4], and novel treatment strategies are needed. Since angiogenesis is a key histopathological feature of neoplasms, inhibitors of new vessel formation (antiangiogenic drugs) are increasingly used in tumor

therapy, typically in combination with other more traditional therapeutic measures such as radiation therapy [5, 6].

At our institution, children with newly diagnosed DIPG are treated with the angiogenesis inhibitor vandetanib in combination with conformal radiation therapy (cRT). However, previous clinical trials have raised concerns that antiangiogenic therapies of brain tumors may increase vessel wall fragility and consequently increase the risk of intratumoral hemorrhage [7–9]. Therefore, patients receive an initial magnetic resonance imaging (MRI) screening and continued monitoring for intracerebral hemorrhages during treatment.

Previously, intratumoral hemorrhages have been assessed by conventional MRI and T2\*-weighted gradient-echo imaging (T2\*-GRE) [10]. More recently, a novel optimized MRI technique, susceptibility-weighted imaging (SWI) has been introduced and has improved our ability to visualize magnetically susceptible substances [11, 12].

The purpose of our study was twofold. First, we compared the standard T2\*-GRE sequence used at our institution with the novel SWI method to better understand its strengths and shortcomings in the detection of intratumoral hemorrhages. Second, we determined the incidence and timely evolution of intratumoral hemorrhages and their potential significance with regard to clinical management.

## Methods

### Study design

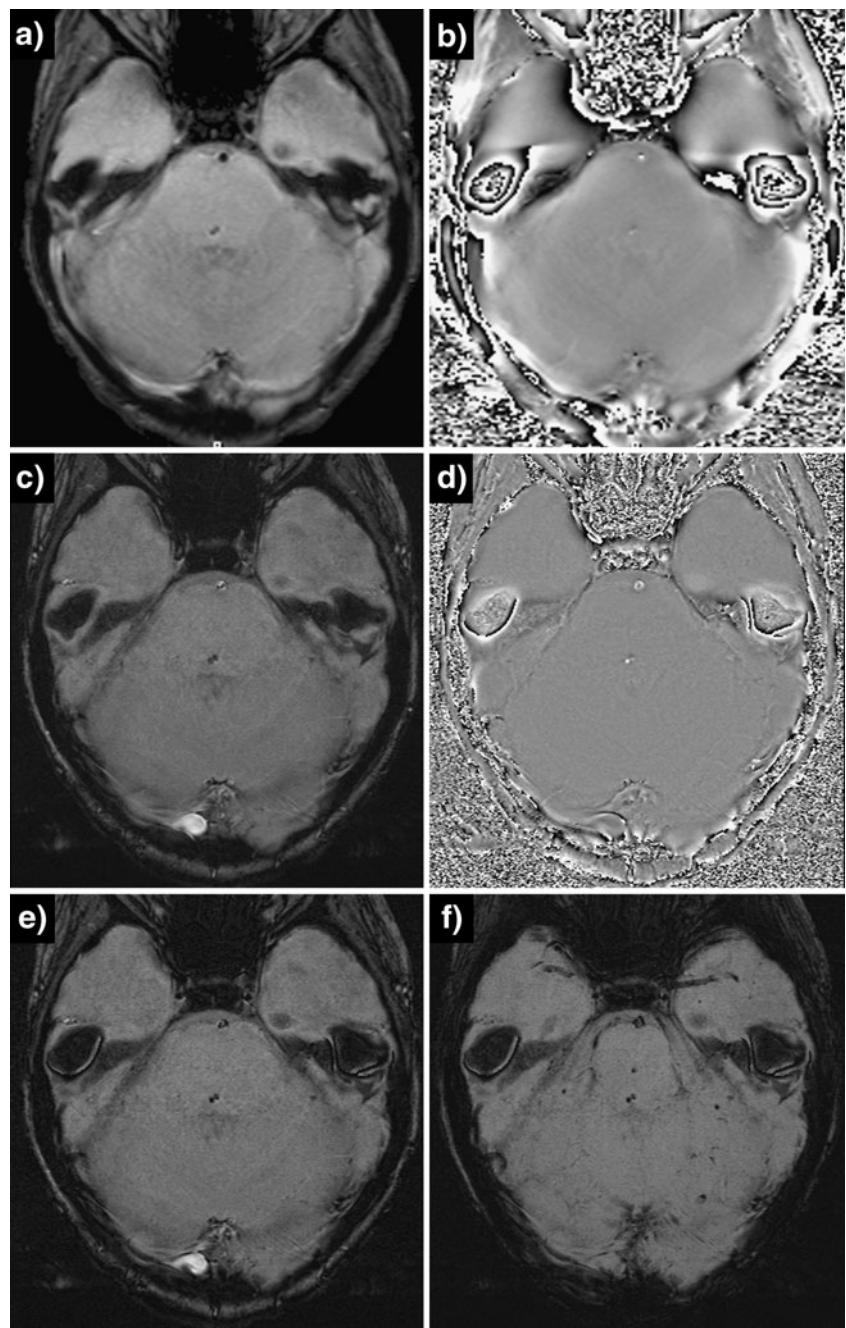
As part of an ongoing clinical phase I trial conducted to estimate the maximum tolerated dose and dose-limiting toxicity of vandetanib (ZD6474, Zactima™, AstraZeneca, Wilmington, DE) when administered in conjunction with cRT in children with newly diagnosed DIPG, we prospectively recruited all patients enrolled between May 2007 and August 2008. Inclusion criteria of the trial were (1) diagnosis of DIPG (or high-grade glioma originating from the brainstem), (2) age between 2 and 21 years at the time of enrollment, and (3) lack of evidence of metastatic disease or intratumoral hemorrhage on conventional MR images. Informed consent, in compliance with guidelines of our institutional review board, was obtained from all patients or their legal guardian prior to enrollment in the study. According to the protocol design, cohorts of 3–6 patients received escalating doses of vandetanib (level 1: 50 mg/m<sup>2</sup>, level 2: 65 mg/m<sup>2</sup>, level 3: 85 mg/m<sup>2</sup>, level 4: 110 mg/m<sup>2</sup>, level 5: 140 mg/m<sup>2</sup>) along with cRT at fractions of 1.8 Gy/day, 5 days/week over a 6-week period (total 54 Gy). Patients received additional supportive medication as deemed appropriate for their clinical condition. However, any concomitant medication that could affect cytochrome P450 3A4 function (except for dexamethasone and fluconazole), or prolong the QT interval or induce torsades de pointes, or both, was avoided.

### MR imaging

All patients underwent a baseline MRI workup at admission. Follow-up scans were performed at 7±3 days, 3 weeks, 6 weeks, then at 2-month intervals, and at the end of treatment. Along with standard MRI sequences, the protocol included T2\*-GRE and SWI sequences. Generally, scans were performed on a 3-T scanner (Magnetom Trio, Siemens Medical Systems; Erlangen, Germany; T2\*-GRE: TR/TE=565/25, matrix 256×192, voxel size 1.1×0.8×4 mm<sup>3</sup>, gap 0.8 mm, 39 slices, averages=2, flip angle 90°, acquisition time 4.35 min; SWI: TR/TE 56/25, matrix 512×253, voxel size 0.6×0.4×2 mm<sup>3</sup>, no gap, 40 slices, averages=1, flip angle 20°, acquisition time 7.51 min). Occasionally, follow-up scans were performed on a 1.5-T machine because of logistic reasons (Magnetom Avanto, Siemens Medical Systems; Erlangen, Germany; T2\*-GRE: TR/TE=1500/33.3, matrix 256×192, voxel size 1.1×0.8×4 mm<sup>3</sup>, no gap, 39 slices, averages=2, flip angle 90°, acquisition time 6.05 min; SWI: TR/TE 54/40, matrix 512×253, voxel size 0.6×0.4×2 mm<sup>3</sup>, no gap, 40 slices, averages=2, flip angle 19°, acquisition time 7.34 min). Parameters of T2\*-GRE and SWI sequences corresponded to the default values used for clinical imaging at our institution. The effect of a lower sensitivity of the SWI sequence to susceptibility at lower field strengths was minimized by a proportionally increasing the echo time used for SWI sequences (see “Discussion” for details). The flip angle of 90° was chosen for T2\*-GRE to saturate the bright signal of the cerebrospinal fluid to an acceptable level in order to improve the diagnostic value of imaging data. Both T2\*-GRE and SWI datasets included magnitude and phase images (Fig. 1). Phase images are essential to differentiate hemorrhage from calcification [13]. Phase data of the T2\*-GRE and SWI were unwrapped to the same extent by homodyne filtering of the complex MRI data during image reconstruction of the MRI system. A 2D Hanning filtered submatrix of the k-space center (25% of the original k-space size) was reconstructed to the original image size by zero filling and used for the homodyne filter by the MRI system.

The major difference between the two susceptibility-sensitive imaging techniques is that T2\*-GRE is a 2D technique and SWI a 3D technique. Because of the larger slices thickness of the 2D sequence small hemorrhages can easily be missed by the T2\*-GRE. For the same reason, the sequence is also more prone to additional signal loss and phase dispersion caused by field inhomogeneities induced by bone-tissue interfaces which are unavoidably around the brain stem. For the SWI technique, SWI maps (obtained by applying a phase mask filter to the magnitude image, which further increases the contrast between susceptible substances and the surrounding tissue) and minimum intensity projection (minIP) images (which increase the conspicuity of susceptibility effects across several partitions) were also available (Fig. 1) [11].

**Fig. 1** T2\*-GRE and SWI images that were used for data evaluation. T2\*-GRE images included magnitude (a) and phase (b) images; SWI included magnitude (c), phase (d), SWI (e), and minimum intensity projection images (f). For both sequences, the image quality was rated as slight susceptibility artifacts or image deformity without interference



#### Definitions and criteria

It is important to note that the appearance of hemorrhage and calcification on phase images depends on the signal encoding and is vendor-specific; therefore, the actual appearance may be inverted on other scanners [14]. In our setting, lesions were considered hemorrhagic on T2\*-GRE and SWI images if there was a central hypointense and hyperintense rim on magnitude images as well as a central hypersignal and hypointense rim on phase images (Fig. 1) [14]. Lesions showing a central hypointense on both magnitude and phase images were interpreted as being

calcified. In concordance with a previous publication [15], lesions 5 mm or larger were defined as “hematomas” and lesions smaller than 5 mm as “petechial” hemorrhages.

#### Data collection

Before data analysis, all T2\*-GRE and SWI image sets were separated and randomized to ensure unbiased analysis. Two reviewers, an MD (Reviewer 1, R1) and a PhD with expertise in SWI imaging (Reviewer 2, R2), scored the number of hemorrhages, taking into account that the same lesion could be conspicuous on adjacent slices. R1 also

measured the diameter of the three largest lesions on magnitude images for both sequences and evaluated the overall image quality by using a modified scoring system as described previously [16–18]. The visibility of hemorrhages was scored as 0: negative, 1: poorly/vaguely visible, 2: visible, but poor delineation, and 3: clearly visible, good delineation. The image quality was scored as 0: severe susceptibility artifacts or image deformity that interfered with interpretation, 1: susceptibility artifacts or image deformity that slightly interfered, 2: slight susceptibility artifacts or image deformity without interference, and 3: no apparent susceptibility artifacts or image deformity. After data collection, all scans were reevaluated by each reviewer, using T2\*-GRE and SWI side by side to identify and resolve misinterpretations of vessels, artifacts, and calcification as hemorrhage. In ambiguous cases, both reviewers reached a consensus in their decision. In addition, an independent, unbiased reviewer, an MD (Reviewer3, R3), assessed all conventional anatomic T1w and T2w images for conspicuity of hemorrhagic lesions without the use of T2\*-GRE and SWI. Reviewers were blinded to dosage data at the time of conducting image analysis.

#### Statistical data analysis

SAS Version 9.1 (SAS Institute Inc., Cary, NC) was used for data analysis. Baseline prevalence and cumulative incidence of hemorrhagic lesions were determined. Because cumulative incidence is estimated continuously over time, and not all patients were scanned at the same time point because of scheduling issues, cumulative incidence was determined at 2, 4, and 6 months after initiation of treatment. Data were analyzed by using descriptive statistics and graphical tools to visually display differences by reviewer and method. The mixed-effects Poisson regression model was used to compare the relative sensitivities of the two methods to detect hemorrhagic lesions, because count data were obtained from each patient in a longitudinal manner. The visibility of hemorrhagic lesions was compared between T2\*-GRE and SWI using Wilcoxon signed rank test.

## Results

### Participants

The 17 consecutive patients (nine female, eight male, age range 3–17 years) included in our evaluation were treated at different dose levels of vandetanib; three patients each received levels 1 to 3, six patients received level 4, and two patients received level 5. The number of available follow-up MR scans for participants varied with time of enrollment and the length of survival (mean 5.4 studies per patient). On four occasions, either T2\*-GRE or SWI was not performed. These

studies were therefore excluded from review. A total of 92 complete studies were available for analysis (one patient received the baseline scan only, two patients had two scans, three patients had four scans, five had six scans, and three patients each had seven and eight scans).

### Type, appearance, and prevalence of lesions

Hemorrhagic lesions were evaluated within the tumor area (only two patients had hemorrhagic lesions outside the tumor). We detected 190 (R1) and 131 (R2) hemorrhagic lesions using T2\*-GRE and 295 (R1) and 280 (R2) hemorrhagic lesions by SWI. The majority of lesions were small petechial hemorrhages, and only 15 hematomas were identified in seven patients by both methods (T2\*-GRE 7.89% [R1] and 11.5% [R2]; SWI 5.08% [R1] and 5.4% [R2]). By using a mixed model and taking interpatient correlation into account, we found that corresponding lesions were significantly smaller ( $P=0.0038$ ) on SWI (range, 0.10–2.56 cm; mean,  $0.30\pm 0.43$  cm) than on T2\*-GRE (range, 0.16–2.66 cm; mean,  $0.39\pm 0.53$  cm). The prevalence of hemorrhages at baseline was 41% [95% confidence interval (CI), 18%, 67%] by T2\*-GRE and 47% (95% CI, 23%, 72%) for SWI. The cumulative incidence at 6 months was 82.4% for T2\*-GRE and 88.2% for SWI. Cumulative incidence did not differ significantly between the two MRI methods ( $P=0.71$ ).

### Effect of time on the occurrence of hemorrhages

There was a significant effect of time on the number of intratumoral hemorrhages. The number of hemorrhages increased during the course of the disease ( $P_{R1}=0.05$ ;  $P_{R2}=0.15$ ), but this increase was not linear. Of the eight patients showing marked increase in the number of hemorrhagic lesions, six had this increase after an initial phase of stability (between 50 and 178 days) (Fig. 2). Of the remaining nine patients, eight were still enrolled in the study and two did not show any hemorrhages during follow-up (follow-up period 287 days for Patient 6 [status: on study] and 53 days for Patient 9 [status: off study]). None of the patients included in this study showed clinically significant neurological deterioration attributable to new hemorrhages; therefore, no patient was excluded from the trial for this reason. Generally, patients were

**Fig. 2** Cumulative incidence of hemorrhagic lesions in patients who showed a marked nonlinear increase in the number of hemorrhagic lesions during the course of the disease. Results of T2\*-GRE scans are displayed in red and those of SWI in black (R1 solid lines, R2 dashed lines). The gray vertical lines represent the time interval of cRT and the red vertical line the point when the patient was taken off the study. The symbol # above the curves marks scans performed on a 1.5-T scanner

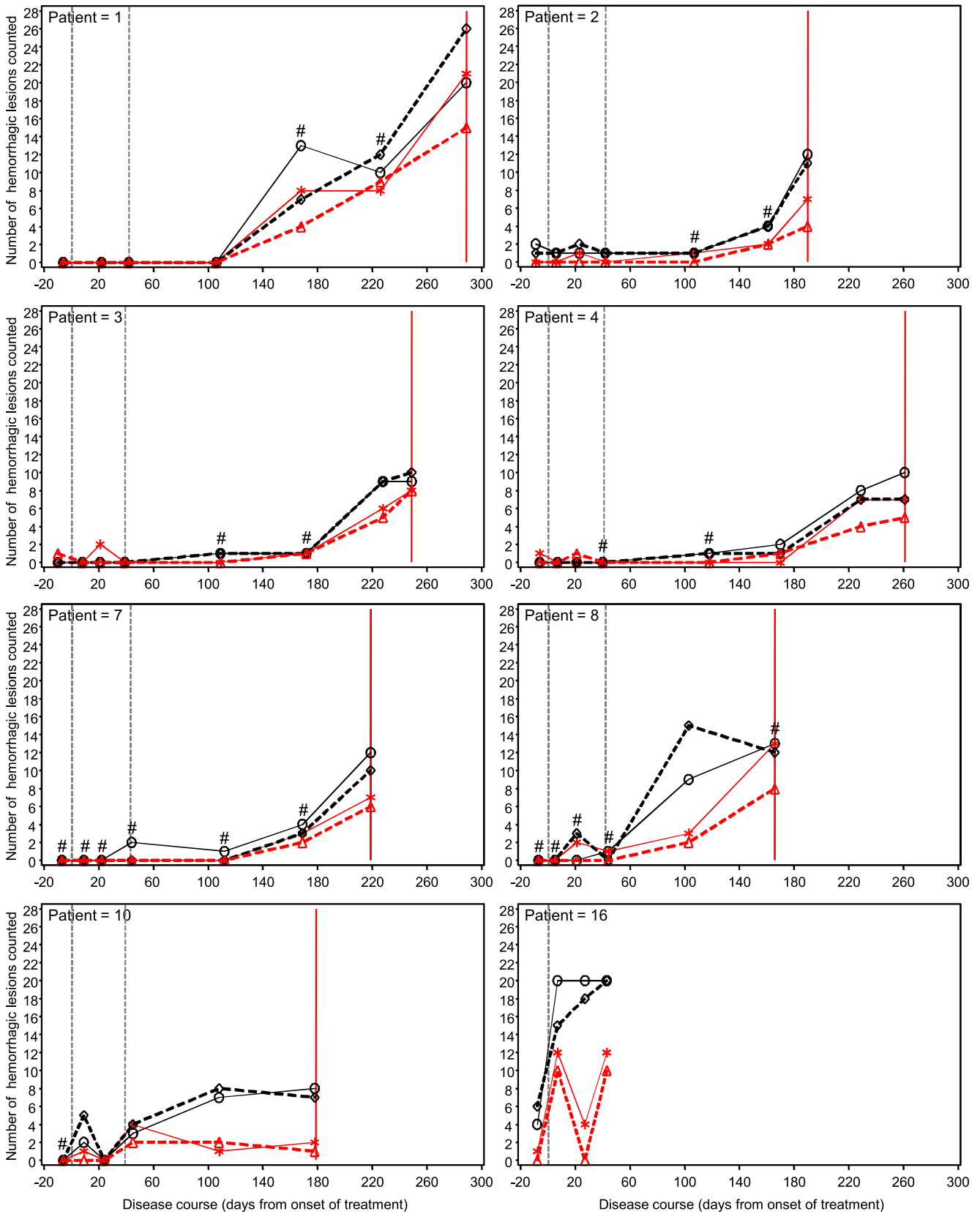
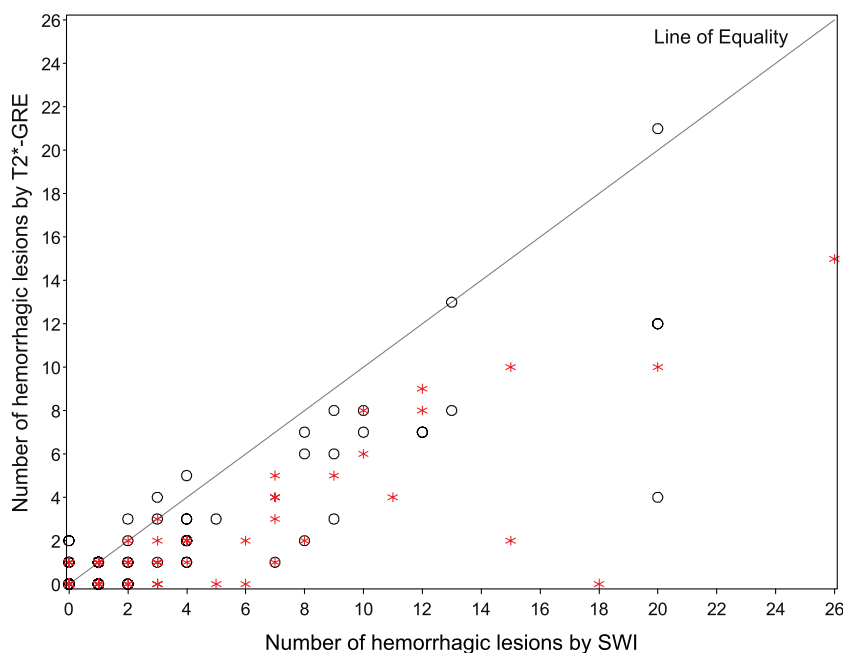


**Fig. 3** Number of hemorrhagic lesions identified by T2\*-GRE and SWI (R1 *black circles*; R2 *red stars*). Each *circle/star* represents the lesion count by T2\*-GRE and SWI of a single patient study



excluded from the research protocol because of progressive disease or fatal outcome.

Detection of hemorrhages by T2\*-GRE and SWI

The number of hemorrhages detected by T2\*-GRE and SWI was the same in 42 (R1, 45.6%) and 43 scans (R2, 46.7%). More lesions were identified by SWI than by T2\*-GRE in 40 (R1, 43.5%) and 42 (R2, 45.6%) scans; conversely, more lesions were identified by T2\*-GRE than SWI in nine (R1, 9.8%) and six (R2, 6.5%) cases (Fig. 3). Differences in the detection of the number of hemorrhages by T2\*-GRE and SWI were statistically significant ( $P_{R1}=0.02$ ;  $P_{R2}<0.001$ ).

The interobserver reliability for detection of hemorrhages was 80% for T2\*-GRE and 91% for SWI (T2\*-GRE  $P=0.11$ ; SWI  $P=0.75$ ). The number of hemorrhagic lesions identified did not have a significantly different trend overtime comparing T2\*-GRE and SWI (the  $p$  values for the time  $\times$  imaging modality interaction were  $P_{R1}=0.34$ ;  $P_{R2}=0.22$ ).

Further consensus evaluation by a side-by-side review of corresponding T2\*-GRE and SWI images revealed that in 28 (R1, 30.4%) and 29 (R2, 31.5%) scans a hemorrhagic lesion was missed and in seven (R1, 7.6%) and 10 (R2, 10.9%) scans vessels, necrotic areas, calcification, or imaging artifacts were misinterpreted as hemorrhage on T2\*-GRE. On the other hand, on SWI images, only one lesion was missed by each reviewer

**Table 1** Criteria for the second (consensus) evaluation of hemorrhages by T2\*-GRE and SWI

Evaluation	No. of lesions Reviewer 1	No. of lesions Reviewer 2
T2*		
Lesion missed on T2*	28	29
Misinterpretation of vessel as lesion on T2*	2	3
Misinterpretation of artifacts as lesion on T2*	3	2
Misinterpretation of lesion as artifact on T2*	0	3
Misinterpretation of necrotic area on T2*	1	1
Misinterpretation of calcification on T2*	1	1
SWI		
Lesion missed on SWI	1	1
Misinterpretation of vessel as lesion on SWI	2	2
Misinterpretation of artifacts as lesion on SWI	4	0
Misinterpretation of lesion as vessel on SWI	1	0
Both		
Counting problematic (necrotic area or high number of hemorrhagic lesions across slices)	15	16
Questionable cases	1	1

The mismatch was attributed to more than one cause in nine (R1) and 10 (R2) scans

**Table 2** Visibility of hemorrhagic lesions by T2\*-GRE and SWI

T2* Visibility	SWI Visibility	No hemorrhage identified	1	2	3	All
No hemorrhage identified						
	0		4	3	4	11
	1	3	2	5	2	12
	2	1		5	16	22
	3			1	13	14
	All	4	6	14	36	60

and in seven (R1, 7.6%) and two (R2, 2.2%) scans vessels or imaging artifacts were misinterpreted as hemorrhagic lesions. In 15 (R1, 16.3%) and 16 (R2, 17.4%) scans, it was difficult to accurately count the hemorrhagic lesions because of their high number across slices or multiple clustered hemorrhages within a presumed intratumoral necrotic area, or both (Table 1).

**Image quality of T2\*-GRE and SWI**

For 60 cases, T2\* or SWI visibility of hemorrhagic lesions was reported (Table 2). In only one case, the visibility on T2\* was higher (2 versus 3) than on SWI. In all other cases, SWI visibility was either as good as T2\* (18 cases) or better (24 cases) than T2\*. Assuming that the scans and patients are independent, Wilcoxon signed rank test also showed this significant difference with  $P < 0.0001$ . The quality of T2\*-GRE images was poorer than that of SWI images. The quality was acceptable (score >0) in 48 T2\*-GRE scans (52.2%) and 72 SWI scans (81.5%) but interfered with confident image evaluation in 44 scans T2\*-GRE (47.8%) and 17 SWI scans (18.5%). Table 3 summarizes the number of hemorrhagic lesions as a function of image quality and the selected phase-encoding direction (for SWI scans only). The quality of scans in which more lesions were identified by SWI was much better than that of scans detected by T2\*-GRE. Also, in scans in which no lesion was identified, image quality did not affect SWI scans but was critical for T2\*-GRE scans, wherein the lack of detectable lesions was likely associated with poor image quality. However, for images in which 1 or

more hemorrhagic lesions were detected, image quality had little effect on the total lesion count with T2\*-GRE, but higher-quality scans allowed identification of more lesions with SWI. On SWI scans, the phase-encoding direction was important for diagnostic accuracy. In the 10 scans for which the phase-encoding direction was set from anterior to posterior, the prevalence of hemorrhagic lesions was lower (50%) than for scans set with the correct phase encoding direction from left to right (63.4%).

Assessment of conventional T1w and T2w images by R3 for conspicuity of hemorrhagic lesions showed that 11 (12%) scans had no evidence of hemorrhage, 30 (32.6%) were classified as unlikely, and 51 (55.4%) as possible hemorrhages. However, no classification was definite.

**Discussion**

A comparison of both susceptibility-sensitive sequences revealed that SWI was more sensitive than T2\*-GRE in detecting intratumoral hemorrhages as well as more specific in differentiating them from mimics and artifacts. The differentiation of hemorrhage from vessels by T2\*-GRE may have been hampered by thick slices, which complicated the tracking of vessels. Also, phase images seemed less reliable for T2\*-GRE than SWI as the example in Fig. 4 illustrates: T2\*-GRE phase images were suggestive of hemorrhage, whereas SWI phase images correctly depicted the presence of calcification. Further studies are required to determine whether this is true for a larger

**Table 3** Number of hemorrhagic lesions as a function of image quality and phase-encoding direction

Reviewer	No. of hemorrhages	Image quality T2*-GRE			Image quality SWI				Phase-encoding direction on SWI	
		0	1	2	0	1	2	3	Wrong	Correct
1	More on SWI	17	10	8	2	13	19	1	3	37
	Matched	3	4	4	2	2	6	1	5	38
	More on T2*	1	4	1	–	2	4	–	2	7
2	More on SWI	18	15	9	2	15	24	1	2	40
	Matched	3	1	4	2	1	4	1	8	36
	More on T2*	–	2	–	–	1	1	–	–	6

Includes only scans that revealed hemorrhages. Phase-encoding direction for SWI scans only

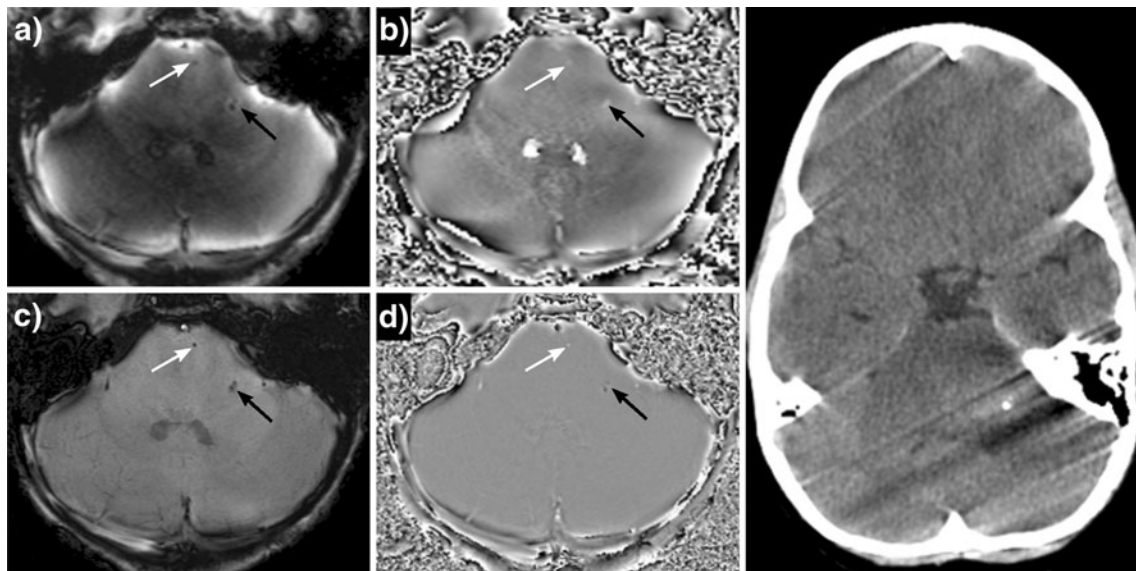


**Fig. 4** Hemorrhage versus calcification. The two index lesions show identical signal properties on both T2\*-GRE magnitude (a) and phase (b) images, suggesting hemorrhagic nature. The SWI magnitude image (c) allows better delineation of the lesions and the corresponding phase

image (d) shows that the lesion within the ventral pons corresponds to a petechial hemorrhage, whereas the lesion within left posterolateral pons is likely a calcification because it exhibits a hyposignal (confirmed by CT)

patient cohort and whether SWI has the potential to universally replace computed tomography in the detection of calcification [19, 20].

Another interesting finding was that, in contrast to T2\*-GRE, SWI may be able to differentiate true hematomas from necrotic areas. Figure 5 shows an area of necrosis that was confirmed by T1w and T2w images. T2\*-GRE images suggest a hemorrhagic lesion within the ventral pons. On SWI magnitude, the hyposignal was less conspicuous and the corresponding phase image did not show a hypersignal,

which formally ruled out the presence of deposits of magnetically susceptible substances within the lesion.

The accidental setting of the phase-encoding direction from anterior to posterior was a potential source of error in SWI images in 1 case. This led to flow artifacts from adjacent vessels to project directly onto the brainstem, which could lead to misinterpretation as hemorrhage on the SWI magnitude image (Fig. 6a). However, the phase image (Fig. 6b) did not show a corresponding hypersignal to indicate a true hemorrhage. If the phase-encoding direction

**Fig. 5** Hemorrhage versus areas of necrosis. T2\*-GRE magnitude (a) and phase (b) images suggest a hemorrhagic lesion within the ventral pons. On SWI magnitude (c), the hyposignal is less conspicuous and the corresponding phase image (d) does not show a hypersignal, which formally rules out the presence of deposits of magnetically susceptible substances within the lesion

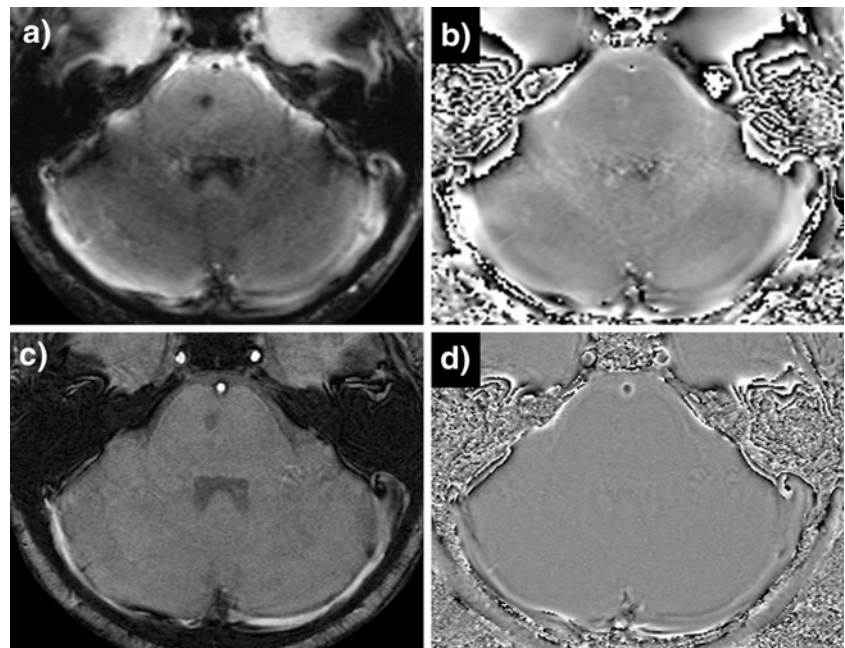
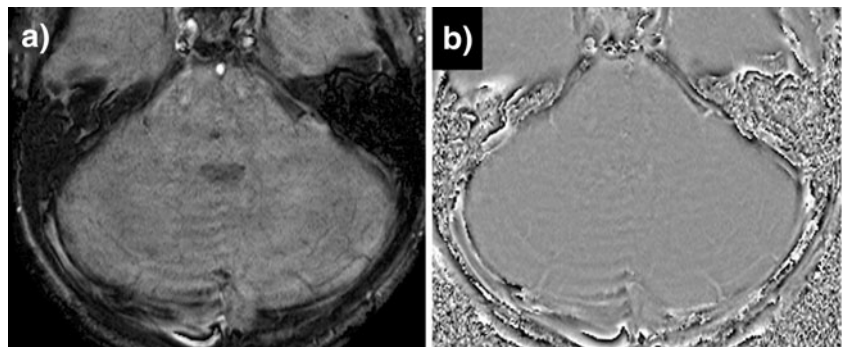




**Fig. 6** SWI images with the phase-encoding direction set from anterior to posterior. Flow artifacts from the basilar artery project directly onto the tumor area on the magnitude image (a) which may lead to misinterpretation. However, the phase image (b) does not show a corresponding hypersignal to indicate a true hemorrhage



is selected appropriately, this potential source of error can be eliminated.

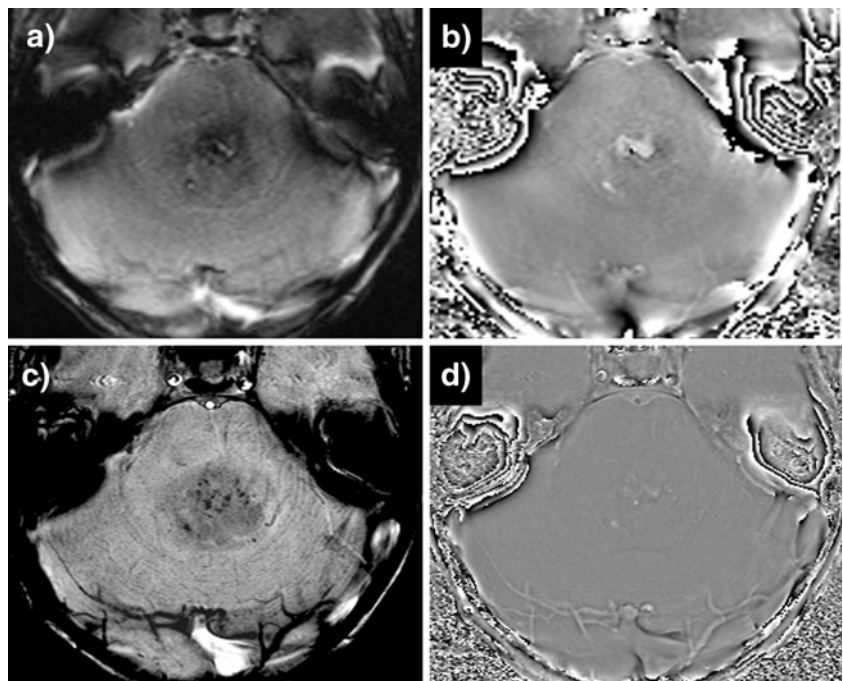
SWI was more sensitive and specific than T2\*-GRE in a technically challenging region such as the posterior fossa, because it was less prone to artifacts, which positively affected the overall image quality and ultimately lesion conspicuity. Although our standard clinical T2\*-GRE sequence may be further optimized by using thinner slices and higher in-plane resolution, the 3D acquisition of SWI data inherently produces better results than those of T2\*-GRE in many respects. For instance, the so-called blooming effect is less prominent on SWI than T2\*-GRE, allowing more accurate identification of size and number of lesions [21]. Figure 7 shows a case wherein lesions apparently corresponding to hematomas on T2\*-GRE images were actually identified as a cluster of petechial hemorrhages by SWI. The only drawbacks of SWI are the longer acquisition time and its limited ability to differentiate between the stages of evolving hemorrhages.

By using the dedicated susceptibility-sensitive MRI techniques T2\*-GRE and SWI, we also found that in our

cohort of children with DIPG treated with the angiogenesis inhibitor vandetanib in conjunction with cRT petechial hemorrhages are more common than previously reported. Nearly 50% of patients presented with at least one intratumoral hemorrhagic focus at diagnosis. Somewhat unexpectedly, true intratumoral hematomas were rare, despite choosing the 5-mm cutoff value to ensure that large potentially neurologically significant lesions within the brainstem are differentiated from smaller ones that are likely clinically irrelevant.

Two factors may have contributed to the higher prevalence of hemorrhages detected in our study. Firstly, previous studies reported the incidence of hemorrhagic lesions by conventional MRI [10, 22–25]. Using mainly T1w and T2w images, the prevalence of lesions at baseline varied from 0% to 26% (compared to 41% by T2\*-GRE and 47% by SWI in our study) [10, 22–25] and the cumulative incidence rate was 15.5% at 6 months (compared to 82.4% by T2\*-GRE and 88.2% by SWI in our study) [22]. Our evaluation also showed that the detection

**Fig. 7** Hematoma versus cluster of petechial hemorrhages. T2\*-GRE magnitude (a) and phase (b) images suggest a hematoma. SWI, magnitude (c), and phase (d) images reveal a cluster of petechial hemorrhages within an area of tumor necrosis



of hemorrhage by T1w and T1w images is uncertain and, therefore, conventional T1w and T2w imaging may be inadequate for the accurate assessment of intratumoral hemorrhagic burden. This underlines the importance of using specific susceptibility-sensitive sequences in patients treated for brain tumors if screening for hemorrhagic complications is clinically warranted or dictated by specific protocol requirements. Second, the higher prevalence of hemorrhages in our study could be treatment related, because the therapy of DIPG in previous studies consisted of cRT only or included other types of chemotherapy [10, 22, 25]. However, the significance of the higher number of hemorrhages and the influence of vandetanib needs to be determined in future studies. The development of cavernous angiomas and/or capillary telangiectasias, which theoretically could account for similar changes on T2\*-GRE and SWI images, is unlikely, taking into account the relatively short period of time post RT. Such lesions have been reported to develop later (2–10 years after radiation) [26].

Our data also suggest that petechial hemorrhages and smaller hematomas may not be clinically relevant in most cases. In other words, contrary to what has been advocated previously [7–9], patients may not need to be excluded or removed from clinical therapeutic trials of angiogenesis inhibitors solely because intratumoral hemorrhages were identified by susceptibility-sensitive sequences. Instead, correlation by neurological finding is required to assess their significance before making clinical management decisions.

Another interesting finding was that a relatively steep increase of intratumoral hemorrhages was observed during the disease course in eight patients after an initial phase of stability (5–178 days). This may be related to a possible rebound effect after an initially successful treatment, a delayed radiation-induced vessel-wall necrosis, or their combination. Also, rapid tumor growth has been shown to increase the incidence of hemorrhages [12], and the presence of susceptibility artifacts within tumors correlates with their histological grade [27]. Increasing intratumoral hemorrhagic diathesis, therefore, may also be an indicator of tumor progression and possible malignant transformation.

Our study is limited by its relatively small patient cohort. Also, not all patients were scanned with the same field strength (1.5 T: 28 exams, 3 T: 64 exams), because of logistic difficulties during the study period. We believe, however, that the inconsistent use of field strength did not influence our results, because the SWI and T2\* contrasts have been found to be almost identical at different field strengths if the echo time is optimized accordingly, as was done in our study [28, 29]. In addition, it has been shown that the contrast index of hemorrhagic lesions on SWI improved only marginally from  $0.67 \pm 0.07$  at 1.5 T to  $0.73 \pm 0.06$  at 3 T [30]. This result suggests a negligible effect of the actual field strength on the

detection of hemorrhagic lesions. The majority of our scans were performed on the 3-T magnet with a maximum of two follow-ups (for 10 of 17 patients) performed on the 1.5-T scanner. In addition, the latest reported scan was performed on the same scanner as the initial study, except for two patients. Therefore, the increase in hemorrhagic lesions over time observed for some patients was not related to the increase in magnetic field strength.

## Conclusion

Our study contributes to a better understanding of the strengths and shortcomings of SWI in imaging of the brain. More specifically, to the best of our knowledge, this is the first study that describes the prevalence and cumulative incidence of intratumoral hemorrhages in DIPG, using dedicated susceptibility-sensitive techniques, and in our cohort, we found that these hemorrhages are more common than previously reported. However, future studies will be needed to determine the influence of various therapies (cRT and angiogenesis inhibitors) on the increasing number of hemorrhages. In addition, the clinical significance of microhemorrhages may need to be further investigated, but our study suggests that these are typically benign and may not warrant discontinuation of antiangiogenic treatment.

**Acknowledgements** This study was supported by American Lebanese Syrian Associated Charities (ALSAC).

The authors wish to thank Vani J. Shanker, PhD, ELS, Department of Scientific Editing, St. Jude Children's Research Hospital, for the many helpful suggestions to improve this manuscript.

**Conflict of interest statement** AstraZeneca provided Dr. Alberto Broniscer with the study medication.

## References

1. CBTRUS (2005) Statistical Report: Primary Brain Tumors in the United States, 1998–2002. Central Brain Tumor Registry of the United States, Chicago
2. Kaatsch P, Rickert CH, Kuhl L, Schuz J, Michaelis J (2001) Population-based epidemiologic data on brain tumors in German children. *Cancer* 92:3155–3164
3. Fischbein NJ, Prados MD, Wara W, Russo C, Edwards MSB, Barkovich AJ (1996) Radiologic classification of brain stem tumors: correlation of magnetic resonance imaging appearance with clinical outcome. *Pediatr Neurosurg* 24:9–23
4. Hargrave D, Bartels U, Bouff  t E (2006) Diffuse brainstem glioma in children: critical review of clinical trials. *Lancet Oncol* 7:241–248
5. Folkman J, Bach M, Rowe JW, Davidoff F, Lambert P, Hirsch C, Goldberg A, Hiatt HH, Glass J, Henshaw E (1971) Tumor angiogenesis - therapeutic implications. *N Engl J Med* 285:1182–1186
6. Folkman J, Klagsbrun M (1987) Angiogenic factors. *Science* 235:442–447

7. MacDonald TJ, Stewart CF, Kocak M, Goldman S, Ellenbogen RG, Phillips P, Lafond D, Poussaint TY, Kieran MW, Boyett JM, Kun LE (2008) Phase I clinical trial of cilengitide in children with refractory brain tumors: pediatric brain tumor consortium study PBTC-012. *J Clin Oncol* 26:919–924
8. Pollack IF, Jakacki RI, Blaney SM, Hancock ML, Kieran MW, Phillips P, Kun LE, Friedman H, Packer R, Banerjee A, Geyer JR, Goldman S, Poussaint TY, Krasin MJ, Wang YF, Hayes M, Murgu A, Weiner S, Boyett JM (2007) Phase I trial of imatinib in children with newly diagnosed brainstem and recurrent malignant gliomas: a pediatric brain tumor consortium report. *Neuro Oncol* 9:145–160
9. Pope WB, Lai A, Nghiemphu P, Mischel P, Cloughesy TF (2006) MRI in patients with high-grade gliomas treated with bevacizumab and chemotherapy. *Neurology* 66:1258–1260
10. Broniscer A, Laningham FH, Kocak M, Krasin MJ, Fouladi M, Merchant TE, Kun LE, Boyett JM, Gajjar A (2006) Intratumoral hemorrhage among children with newly diagnosed, diffuse brainstem glioma. *Cancer* 106:1364–1371
11. Reichenbach JR, Haacke EM (2001) High-resolution BOLD venographic imaging: a window into brain function. *NMR Biomed* 14:453–467
12. Tong KA, Ashwal S, Obenaus A, Nickerson JP, Kido D, Haacke EM (2008) Susceptibility-weighted MR imaging: a review of clinical applications in children. *AJNR Am J Neuroradiol* 29:9–17
13. Gronemeyer SA, Langston JW, Hanna SL (1992) MR imaging detection of calcified intracranial lesions and differentiation from iron-laden lesions. *J Magn Reson Imaging* 2:271–276
14. Deistung A, Mentzel HJ, Rauscher A, Witoszynskij S, Kaiser WA, Reichenbach JR (2006) Demonstration of paramagnetic and diamagnetic cerebral lesions by using susceptibility weighted phase imaging (SWI). *Z Med Phys* 16:261–267
15. Kidwell CS, Wintermark M (2008) Imaging of intracranial haemorrhage. *Lancet Neurol* 7:256–267
16. Akter M, Hirai T, Hiai Y, Kitajima M, Komi M, Murakami R, Fukuoka H, Sasao A, Toya R, Haacke EM, Takahashi M, Hirano T, Kai Y, Morioka M, Hamasaki K, Kuratsu J, Yamashita Y (2007) Detection of hemorrhagic hypointense foci in the brain on susceptibility-weighted imaging clinical and phantom studies. *Acad Radiol* 14:1011–1019
17. Liang LX, Korogi Y, Sugahara T, Shigematsu Y, Okuda T, Ikushima I, Takahashi M (1999) Detection of intracranial hemorrhage with susceptibility-weighted MR sequences. *Am J Neuroradiol* 20:1527–1534
18. Sehgal V, Delproposto Z, Haddar D, Haacke EM, Sloan AE, Zamorano LJ, Barger G, Hu J, Xu Y, Prabhakaran KP, Elangovan IR, Neelavalli J, Reichenbach JR (2006) Susceptibility-weighted imaging to visualize blood products and improve tumor contrast in the study of brain masses. *J Magn Reson Imaging* 24:41–51
19. Wu Z, Mittal S, Kish K, Yu Y, Hu J, Haacke EM (2009) Identification of calcification with MRI using susceptibility-weighted imaging: a case study. *J Magn Reson Imaging* 29:177–182
20. Zhu WZ, Qi JP, Zhan CJ, Shu HG, Zhang L, Wang CY, Xia LM, Hu JW, Feng DY (2008) Magnetic resonance susceptibility weighted imaging in detecting intracranial calcification and hemorrhage. *Chin Med J (Engl)* 121:2021–2025
21. Tong KA, Ashwal S, Holshouser BA, Nickerson JP, Wall CJ, Shutter LA, Osterdock RJ, Haacke EM, Kido D (2004) Diffuse axonal injury in children: clinical correlation with hemorrhagic lesions. *Ann Neurol* 56:36–50
22. Hargrave D, Chuang N, Bouffet E (2008) Conventional MRI cannot predict survival in childhood diffuse intrinsic pontine glioma. *J Neurooncol* 86:313–319
23. Kaplan AM, Albright AL, Zimmerman RA, Rorke LB, Li H, Boyett JM, Finlay JL, Wara WM, Packer RJ (1996) Brainstem gliomas in children—A Children’s Cancer Group review of 119 cases. *Pediatr Neurosurg* 24:185–192
24. Packer RJ, Boyett JM, Zimmerman RA, Rorke LB, Kaplan AM, Albright AL, Selch MT, Finlay JL, Hammond GD, Wara WM (1993) Hyperfractionated radiation therapy (72 Gy) for children with brain stem gliomas. A childrens cancer group phase I/II trial. *Cancer* 72:1414–1421
25. Smith RR, Zimmerman RA, Packer RJ, Hackney DB, Bilaniuk LT, Sutton LN, Goldberg HI, Grossman RI, Schut L (1990) Pediatric brainstem glioma. Post-radiation clinical and MR follow-up. *Neuroradiology* 32:265–271
26. Koike S, Aida N, Hata M, Fujita K, Ozawa Y, Inoue T (2004) Asymptomatic radiation-induced telangiectasia in children after cranial irradiation: frequency, latency, and dose relation. *Radiology* 230:93–99
27. Bagley LJ, Grossman RI, Judy KD, Curtis M, Loevner LA, Polansky M, Detre J (1997) Gliomas: correlation of magnetic susceptibility artifact with histologic grade. *Radiology* 202:511–516
28. Deistung A, Rauscher A, Sedlacik J, Stadler J, Witoszynskij S, Reichenbach JR (2008) Susceptibility weighted imaging at ultra high magnetic field strengths: theoretical considerations and experimental results. *Magn Reson Med* 60:1155–1168
29. Sedlacik J, Kutschbach C, Rauscher A, Deistung A, Reichenbach JR (2008) Investigation of the influence of carbon dioxide concentrations on cerebral physiology by susceptibility-weighted magnetic resonance imaging (SWI). *Neuroimage* 43:36–43
30. Nandigam RN, Viswanathan A, Delgado P, Skehan ME, Smith EE, Rosand J, Greenberg SM, Dickerson BC (2009) MR imaging detection of cerebral microbleeds: effect of susceptibility-weighted imaging, section thickness, and field strength. *AJNR Am J Neuroradiol* 30:338–343